A model of cardiac ryanodine receptor gating predicts experimental Ca^{2+}-dynamics and Ca^{2+}-triggered arrhythmia in the long QT syndrome

Dan Wilson, Bard Ermentrout, Jan Němec, and Guy Salama

Citation: Chaos **27**, 093940 (2017); doi: 10.1063/1.5000711
View online: https://doi.org/10.1063/1.5000711
View Table of Contents: http://aip.scitation.org/toc/cha/27/9
Published by the American Institute of Physics

A model of cardiac ryanodine receptor gating predicts experimental Ca^{2+}-dynamics and Ca^{2+}-triggered arrhythmia in the long QT syndrome

Dan Wilson,[1] Bard Ermentrout,[1] Jan Němec,[2,a)] and Guy Salama[2,b)]
[1]*Department of Mathematics, University of Pittsburgh, Pittsburgh, Pennsylvania 15261, USA*
[2]*Department of Medicine, Heart and Vascular Institute, University of Pittsburgh, Pittsburgh, Pennsylvania 15261, USA*

(Received 10 April 2017; accepted 17 August 2017; published online 26 September 2017)

Abnormal Ca^{2+} handling is well-established as the trigger of cardiac arrhythmia in catecholaminergic polymorphic ventricular tachycardia and digoxin toxicity, but its role remains controversial in Torsade de Pointes (TdP), the arrhythmia associated with the long QT syndrome (LQTS). Recent experimental results show that early afterdepolarizations (EADs) that initiate TdP are caused by spontaneous (non-voltage-triggered) Ca^{2+} release from Ca^{2+}-overloaded sarcoplasmic reticulum (SR) rather than the activation of the L-type Ca^{2+}-channel window current. In bradycardia and long QT type 2 (LQT2), a second, non-voltage triggered cytosolic Ca^{2+} elevation increases gradually in amplitude, occurs before overt voltage instability, and then precedes the rise of EADs. Here, we used a modified Shannon-Puglisi-Bers model of rabbit ventricular myocytes to reproduce experimental Ca^{2+} dynamics in bradycardia and LQT2. Abnormal systolic Ca^{2+}-oscillations and EADs caused by SR Ca^{2+}-release are reproduced in a modified 0-dimensional model, where 3 gates in series control the ryanodine receptor (RyR2) conductance. Two gates control RyR2 activation and inactivation and sense cytosolic Ca^{2+} while a third gate senses luminal junctional SR Ca^{2+}. The model predicts EADs in bradycardia and low extracellular $[K^+]$ and cessation of SR Ca^{2+}-release terminate salvos of EADs. Ca^{2+}-waves, systolic cell-synchronous Ca^{2+}-release, and multifocal diastolic Ca^{2+} release seen in subcellular Ca^{2+}-mapping experiments are observed in the 2-dimensional version of the model. These results support the role of SR Ca^{2+}-overload, abnormal SR Ca^{2+}-release, and the subsequent activation of the electrogenic Na^+/Ca^{2+}-exchanger as the mechanism of TdP. The model offers new insights into the genesis of cardiac arrhythmia and new therapeutic strategies. *Published by AIP Publishing.* [http://dx.doi.org/10.1063/1.5000711]

The manuscript represents an important advance in the field of cardiac arrhythmia mechanisms, with respect to how abnormalities in Ca^{2+} dynamics can lead to arrhythmias. Abnormalities in Ca^{2+} handling, Ca^{2+} overload, and spontaneous Ca^{2+} release from the sarcoplasmic reticulum (SR) have been implicated as a mechanism that initiates and sustains arrhythmias in a wide range of pathologies, including heart failure, ischemic myopathy, bradycardia, and long QT syndrome. However, no study has explained how spontaneous SR Ca^{2+} release which is thought to be a random process at Ca^{2+} release units can elicit sufficient membrane depolarization to activate an electrical pulse that can capture and propagate "out-of-phase" to trigger an arrhythmia. With novel optical mapping techniques (high temporal resolution and high spatial (subcellular) resolution), we showed that spontaneous SR Ca^{2+} release can occur synchronously from the Ca^{2+} release units of multiple cells (~1 mm diameter zones) at the base of the heart.[1] Synchronization occurs when Ca^{2+} is elevated simultaneously in the dyadic space outside the SR and in the luminal space inside the junctional SR. These findings brought compelling evidence as to how abnormal Ca^{2+} dynamics can elicit arrhythmias. Here, we modified a computational model of the rabbit heart action potential and Ca^{2+} handling to show how intracellular calcium overload can result in synchronous SR Ca^{2+} release. The new model requires a more detailed description of the gating properties of cardiac ryanodine receptor (RyR2), the channel responsible for SR Ca^{2+} release. RyR2 is modeled as a channel with 3 Ca^{2+} sensing gates: an activation gate and an inactivation gate on the dyadic side of the SR membrane and an activation gate on the luminal side of RyR2. This description of RyR2 gating is essential to recapitulate the experimental data and is in agreement with new experimental data on the regulation of RyR2 by luminal SR Ca^{2+}. The simulation reinforce the experimental data, explains synchronization of SR Ca^{2+} release, and contributes in a fundamental way as to the Ca^{2+} dependent gating of RyR2.

INTRODUCTION

The heart consists of billions of myocytes which contract synchronously for the heart to function as a pump. In each myocyte, a contraction is triggered by an increase of free Ca^{2+} in the cytoplasm to activate the contractile apparatus. Contractions among myocytes are synchronized by the rapidly propagating wave of membrane depolarization, called the action potential (AP). The membrane

a)Dedicated to the Memory of our dearest friend and colleague Dr. Jan Nemec.
b)Author to whom correspondence should be addressed: gsalama@pitt.edu. Tel.: 412 648–9354. FAX: 412 648–5991.

depolarization opens voltage-gated L-type Ca^{2+} channels located on T-tubules of myocytes resulting in a Ca^{2+} current, $I_{Ca,L}$, and Ca^{2+} influx from the extracellular fluid into the cell. The impulse of Ca^{2+} injected in narrow clefts between the T-tubule and the sarcoplasmic reticulum (SR) triggers the opening of SR Ca^{2+}-release channels, known as cardiac ryanodine receptors (RyR2) and the release of Ca^{2+} stored in the SR.[2] The process of opening RyR2 and releasing Ca^{2+} from the SR caused by the AP and the injection of Ca^{2+} via $I_{Ca,L}$ is known as calcium-induced calcium release (CICR).[3,4] Relaxation is caused by the removal of Ca^{2+} ions from the cytoplasm back into the SR and into the extracellular fluid by the NCX current, I_{NCX}.

Conditions where Ca^{2+} influx and efflux are not in balance as in tachycardia or bradycardia result in electromechanical abnormalities such as electromechanical alternans[5,6] and repolarization delays, respectively;[7] extreme changes in rate are arrhythmogenic. Besides rate changes, mutations of ion channels or transport systems alter the balance between influx and efflux of ions, disturbing the mechanisms coupling membrane potential to Ca^{2+} cycling also causing cardiac arrhythmias. For example, in patients with catecholaminergic polymorphic ventricular tachycardia (CPVT), mutations of RyR2 or calsequestrin result in spontaneous openings of RyR2, non-voltage triggered SR Ca^{2+} release during diastole that depolarize the cell membrane by augmenting NCX activity (an event termed delayed afterdepolarization; DAD), and occasionally cause life-threatening ventricular tachycardia.[8–10] A similar mechanism is responsible for arrhythmias related to digoxin toxicity[11,12] and perhaps in some forms of heart failure.[13]

Repolarization delays due to bradycardia, prolongation of the QT interval or of ventricular AP duration (APD) can lead to abnormal Ca^{2+} dynamics and potentially lethal arrhythmias. A number of conditions lead to Long QT syndrome (LQTS):[14] (i) inherited mutation of one of many genes that encode for cardiac ion channel subunits or interacting proteins (congenital LQTS; cLQTS) or (ii) to acquired conditions such as drug toxicity or electrolyte abnormality (acquired LQTS; aLQTS).[15] Both conditions are associated with sudden cardiac death due to a specific form of ventricular arrhythmia called *Torsade de Pointes* (TdP).[16] TdP is associated with secondary depolarization events occurring during the plateau phase of the AP; that is, depolarizations that occur after the AP upstroke and before repolarization and called as early afterdepolarization (EAD). The mechanism of EAD generation is disputed and two hypotheses dominate the current literature. The first hypothesis postulates that during long AP plateaus, the membrane potential falls in the range corresponding to L-type Ca^{2+} channel window current (i.e., the range of voltage where neither the activation nor the inactivation voltage gates are fully closed) resulting in membrane depolarization due to the reopening of the L-type channels.[17–19] The second hypothesis is that long QT leads to intracellular Ca^{2+}-overload, abnormal SR Ca^{2+}-release during systole, which in turn activates a depolarizing NCX current, and the reactivation of L-type Ca^{2+}-channels.[20,21] The two mechanisms differ in a fundamental way: the first posits that the EAD elicits a second SR Ca^{2+} in systole and the second that spontaneous (non-voltage-triggered) SR Ca^{2+} release elicits EADs.

Recent studies have investigated subcellular Ca^{2+} dynamics from cells in intact perfused hearts and compared their properties in different regions of the epicardium.[1,7,21–24] In Langendorff perfused hearts with aLQTS and bradycardia, a secondary systolic Ca^{2+} elevation gradually develops in myocytes from the base but not the apex of epicardium. Several experimental results support the notion that EADs require a condition for SR Ca^{2+} overload and spontaneous (non-voltage-triggered): SR Ca^{2+}-release and a secondary cytosolic Ca^{2+} elevation temporally precede EADs. A novel dual Ca^{2+} and voltage imaging technique with high spatial (1.5×1.5 μm^2) and temporal (500 frames/s) resolution revealed that spontaneous SR Ca^{2+} release occurs synchronously in regions of ~0.5 mm in diameter that can overcome the source-sink mismatch and initiate TdP.[1,7] Bradycardia-related EADs and TdP were suppressed with the RyR2 stabilizer K201 at low concentrations (0.5 μM) to avoid its possible off-target effects.[7] These measurements provide compelling evidence that abnormal Ca^{2+} dynamics rather than L-type window current drives EADs and TdP in bradycardia and aLQT2.

Experimentally, the finding of SR Ca^{2+} release synchronization within myocytes and among adjacent myocytes is essential to initiate TdP. Yet, what is the mechanism that synchronizes SR Ca^{2+} release from thousands of release units with a cell? And why do hundreds of adjacent cells on the epicardium also synchronize their SR Ca^{2+} release? In the absence of Ca^{2+} cycling pathology, a high concentration of Ca^{2+} in the cytosol and the lumen of the SR appear to be the most plausible explanation. The complexity of Ca^{2+} dynamics and its cross-talk with electrical events make computer simulations a natural tool to further dissect these problems. However, we are not aware of a mathematical model that could provide even a qualitative description of EAD generation in LQTS due to abnormal SR Ca^{2+} release.

In the work presented here, we have modified the Shannon-Puglisi-Bers (SPB) model[25,26] of rabbit ventricular myocyte in a way that reproduces many of the observations previously reported in optical mapping experiments. When this spatially 0-dimensional model is extended to 2 dimensions, it reproduces the subcellular Ca^{2+} dynamics measure by dual optical mapping of APs and Ca^{2+} transients, including propagated intracellular calcium waves during diastole, secondary systolic calcium release which is cell-synchronous, and the occasionally observed behavior with multiple interacting calcium waves.[1,22] The model offers additional insights into the mechanisms of EAD generation and might be useful in the development of new TdP management strategies.

METHODS

The original SPB zero-dimensional (0-D) model has been modified in 2 steps. First, we modified the equations describing intracellular Ca^{2+} handling. Second, we created a 2-D version of the modified SPB 0-D model to simulate the contrasting processes of propagating diastolic Ca^{2+} waves,

and the highly synchronous secondary Ca^{2+} release occurring during systole when repolarization is impaired.

0-D model

The intracellular Ca^{2+} dynamics of the SPB model has been modified in 2 major ways. The SR compartment has been divided into diffusively coupled junctional and non-junctional SR sub-divisions (JSR and NSR) to reflect the fact that most of the SR Ca^{2+}-release occurs from the JSR, but most of the uptake takes place in the NSR [Fig. 1(a)].[27,28] We also changed the description of RyR2, the JSR Ca^{2+} release channel, from the Markovian formalism to a system of 3 serially coupled gates to describe the channel properties of RyR2. Gate 1 controls the rapid RyR2 channel activation as a function of increasing Ca^{2+} in the dyadic space (g1),[3,4]

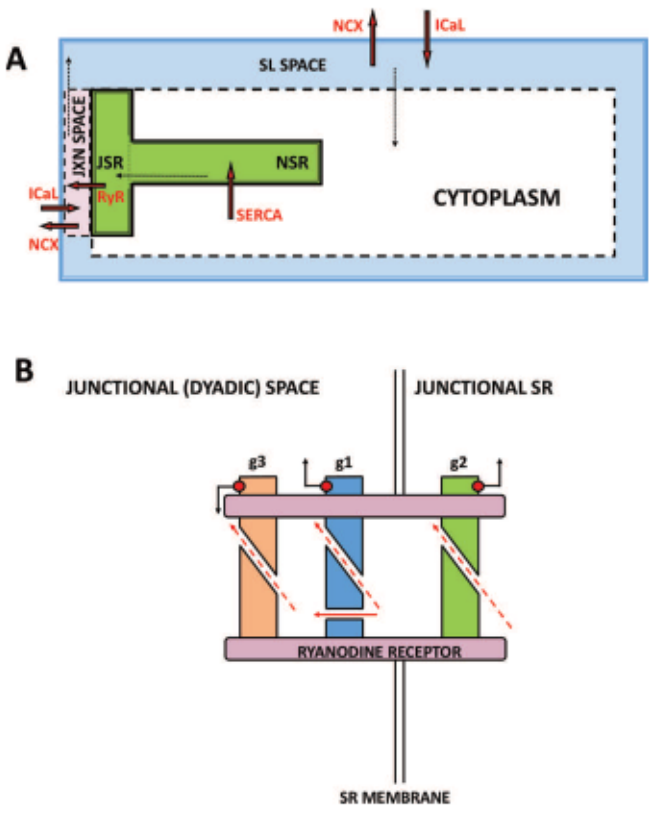

FIG. 1. Simplified diagram of the 0-dimensional version of the model. (a) Similar to the SPB model, the cell volume is divided into cytoplasm, subsarcolemmal (**SL**), and dyadic or junctional (**JXN**) compartments. In contrast to the SPB model, sarcoplasmic reticulum consists of junctional (**JSR**) and nonjunctional (**NSR**) spaces. The simple diffusion coupling between compartments is indicated by dashed arrows. Active transport of Ca^{2+} ions (**SERCA**, **NCX**) and Ca^{2+} ion channels (**RyR**, **ICaL**) are marked by red arrows. The model assumes that SERCA is only present in NSR and RyR2 only in JSR. The NCX and I_{CaL} transport Ca^{2+} between extracellular space and both SL and JXN compartments. (b) The ryanodine receptor is modeled with 3 serial gates (**g1**, **g2**, and **g3**). All gates are affected by Ca^{2+} binding (red circles), which increases open probability of g1 and g2 (up arrows) and decreases open probability of g3 (down arrow). The g1 gate responds to Ca^{2+} concentration in junctional space; g2 responds to calcium in JSR. A small diffusional leak (solid red arrow through g1) in parallel to g1 allows for RyR2 opening by high Ca^{2+} in JSR even in the absence of Ca^{2+} in JXN space. Inactivation of RyR2 by prolonged exposure to high Ca^{2+} concentration in JXN space is modeled by g3. The time-constant of g3 response is an order of magnitude longer (hundreds of ms) than the time-constants of g1 and g2 response.

gate 3 is a slower inactivation controlled by persistently elevated Ca^{2+} in the same compartment (g3), and gate 2 controls the channel opening/activation as a function of elevated Ca^{2+} in the JSR (g2)[29–31] [Fig. 1(b)]. Because we are interested in preserving both CICR and RYR2 opening as a function of high luminal calcium, we choose to model the RyR2 gates using equations similar to the Hodgkin-Huxley formalism (HH) rather than considering the opening of individual RyR2 via a Markovian process. While the underlying dynamics of RyR2 opening are stochastic, it is well established that deterministic equations can be used to model the aggregate behavior provided that there are enough ionic channels.[32,33] Each gate has a steady-state value governed by the free Ca^{2+} concentration in the relevant compartment (i.e., JSR for g2 and junctional space for g1 and g3) and described by a Hill equation. The time constant for g1 is substantially shorter than that of g3 (20 and 300 ms in the data reported here), so that an elevation of Ca^{2+} in the junctional space (JXN) would open RyR2 before eventually closing it. In order to reproduce RyR2 opening by high Ca^{2+} concentration in JSR in the absence of Ca^{2+} in the junctional space, a small diffusion-driven Ca^{2+} leak is placed in parallel to the g1 gate. Its magnitude (model parameter **B**) was between 0.0005 and 0.05 of the maximum g1 permeability in different model runs.

The model was run with MATLAB 2016b. The code was created by modification of the SPB MATLAB code kindly provided by Dr. Puglisi. The code uses the MATLAB **ode15s** procedure to solve the system of multiple ordinary differential equations describing the SPB model, with the relative error tolerance parameter set to 10^{-8}.

2-D model

The 2-D model represents a discretized version of the 0-D model into N compartments of equal size. We assume that the dynamics of each compartment are governed a set of equations identical to the 0-D model, except for the following differences: all cellular currents and junctional, subsarcolemmal, cytoplasmic, and SR volumes are decreased by a factor of 1/N. Furthermore, the rate of change of the cellular voltage is taken to be the sum of the currents from each compartment; spatial voltage gradients were not considered. As emphasized in Fig. 2, 2D simulations included isotropic, diffusive coupling between adjacent SL and adjacent cytoplasmic calcium compartments. Coupling between SL compartments reflects higher calcium concentrations proximal to a RyR2 following each opening which can diffuse to neighboring RyR2 and result in CICR. RyR2 Spatial heterogeneity was considered in various simulations by incorporating variation in the parameters corresponding to the g1 RyR2 gate. In all 2-D simulations, a $L \times W = 50 \times 20$ array of compartments was simulated, where L and W are the length and width, respectively.

2-D numerical simulations were performed on NVIDIA Geforce GTX 1080 graphics cards using the CUDA programming language.[34] Gating variables were updated at each time step using a Rush-Larsen[35] scheme, with the remaining variables updated using a Forward-Euler scheme. A fixed time step of $dt = 0.004$ ms was used in all 2-D simulations.

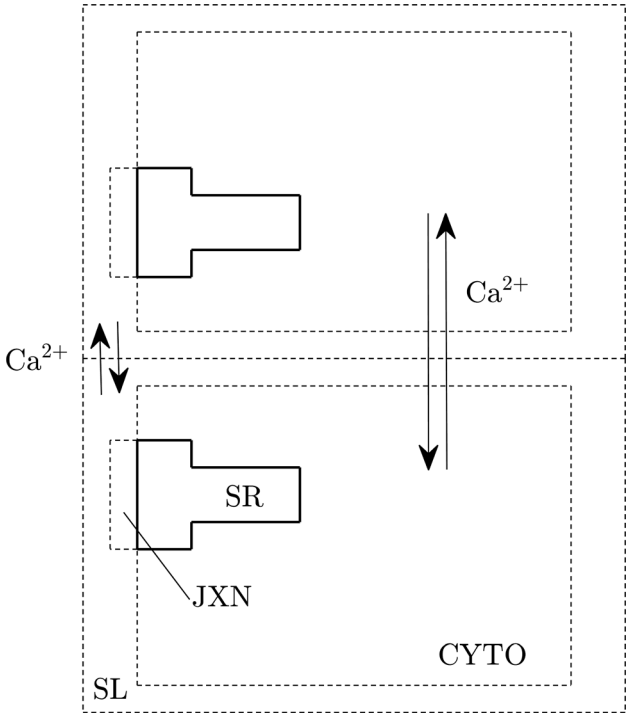

FIG. 2. Simplified diagram of the 2-dimensional model. In the 2-dimensional model, each compartment is assumed to have a lumped SL, JXN, SR, and cytosolic space, with the majority of dynamics governed by the 0-dimensional equations; key differences are explained in the text. Isotropic Ca^{2+} diffusion is assumed between SL to SL and cytosol to cytosol in all adjacent compartments.

The resulting numerical model is stiff, i.e., with a time step dictated by numerical stability requirements. Reducing the time step does not have a significant impact on the resulting model behavior.

RESULTS

0-D model

Several variants of the spatially 0-dimensional model were tested to reproduce the salient features of optical experiments obtained in the Langendorff model of LQTS.[1,22] In particular, the model's parameters were modified to obtain secondary systolic increase in the cytoplasmic Ca^{2+} associated with EADs, bradycardia-dependent EADs, and arrhythmia dependent on Ca^{2+} cycling. Unless stated otherwise, the model was paced by 1 ms current injections with regular cycle length, ranging from 400 ms to 1700 ms. In order to simulate the gradual onset of pharmacological I_{Kr} block in the Langendorff experiments, the model would be run for 5 s with nominal parameters, after which the ***gkr*** parameter (describing the maximal I_{Kr} current density) would be decreased to 10% of the initial value over 30 s using a linear ramp function and left unchanged after that too [Fig. 3(g)].

Similar to experimental observation, this resulted in an initial appearance of a single EAD per AP, followed by the appearance of double EADs and eventually multiple EADs per AP [Fig. 3(a)], which are thought to lead to TdP in multicellular experiments. The EADs were accompanied by secondary systolic elevations of cytosolic Ca^{2+}. In the model,

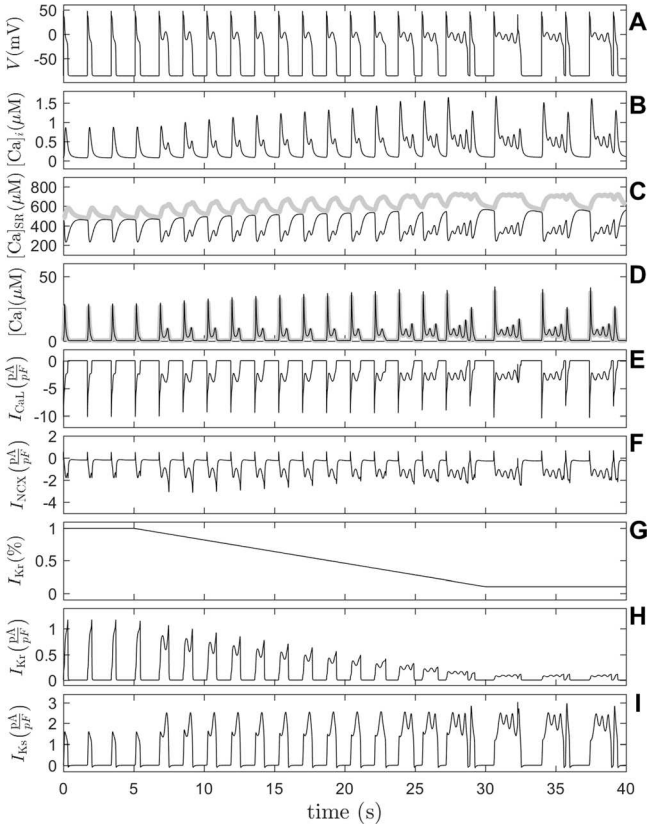

FIG. 3. The 0-D model reproduces gradual development of EADs and EAD salvos (pacing at 1700 ms and gradual I_{Kr} block. Simultaneous plots of selected model variables. (a) Membrane voltage. (b) Free Ca^{2+} concentration in cytoplasmic compartment. (c) Free Ca^{2+} concentration for junctional SR (black) and nonjunctional SR (grey). (d) Free Ca^{2+} concentration for subsarcolemmal space (grey) and junctional space (black). (e) and (f) I_{CaL} and I_{NCX} currents, respectively, Inward currents are assigned negative sign. (g) Time-course of imposed I_{Kr} block. The gradual onset of pharmacological I_{Kr} block in a perfused rabbit heart experiments is modeled as a linear ramp starting from nominal I_{Kr} amplitude after 5 s of model run and terminating at 10% of the nominal value 30 s later. (h) and (i) I_{Kr} and I_{Ks} currents, respectively. Note the secondary spikes of Ca^{2+} concentration in junctional, sarcolemmal, and cytoplasmic spaces, and the gradual increase of Ca^{2+} both in SR compartments and in the cytoplasm.

systolic Ca^{2+} elevations were preceded by RyR2 openings and rise of Ca^{2+} in the JXN and SL compartments [Figs. 3(b)–3(d)]. They were accompanied by the increase in the I_{CaL} and I_{NCX} inward currents [Figs. 3(e) and 3(f)], which were partially compensated by the increase in the outward currents I_{Kr} and I_{Ks} [Figs. 3(h) and 3(I)]. The increase in the pacing rate delayed the onset, or—with short enough cycle length—eliminated the appearance of secondary Ca^{2+} oscillations and EADs (Fig. 4). Decreased Ca^{2+} concentration in JSR and increased outward current, I_{Ks} [Figs. 4(g) and 4(h)] contribute to the disappearance of EADs during faster pacing. Under voltage clamp conditions, EADs can be eliminated by the voltage-clamp but spontaneous SR Ca^{2+} elevation still remain (Fig. 5). Hence, secondary systolic Ca^{2+} elevations are not triggered by EADs, are independent of membrane potential and of Ca^{2+} injection in the cell through L-type Ca^{2+} channels, and hence are caused by spontaneous SR Ca^{2+} release.

Various modifications of the model were explored to investigate the causality of the changes in membrane

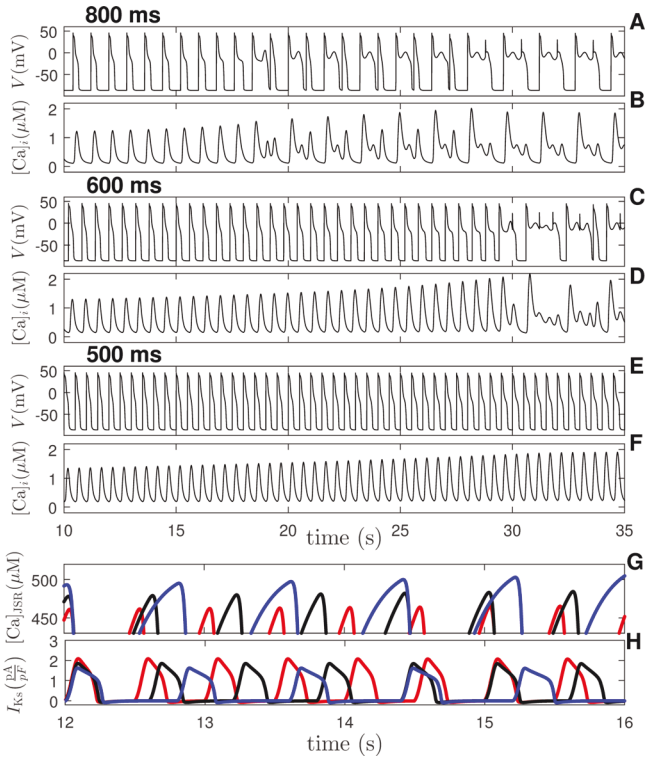

FIG. 4. Promotion of EADs by slow pacing is reproduced by the model. Compared with pacing at 800 ms [panels (a) and (b)], pacing at 600 ms [panels (c) and (d)] delays and pacing at 500 ms [panels (e) and (f)] abolish the onset of EADs. The I_{Kr} block is same as in Fig. 3. Panels (a), (c), and (e) show membrane voltage, and panels (b), (d), and (f) show cytoplasmic Ca^{2+}. In panels (g) and (h), red, black, and blue traces correspond to trials with 500, 600, and 800 ms pacing rates. In panel (g), concentrations of Ca^{2+} in JSR immediately preceding emptying are elevated during slower pacing. In panel (h), outward current, I_{Ks}, is reduced during slower pacing which contributes to APD prolongation.

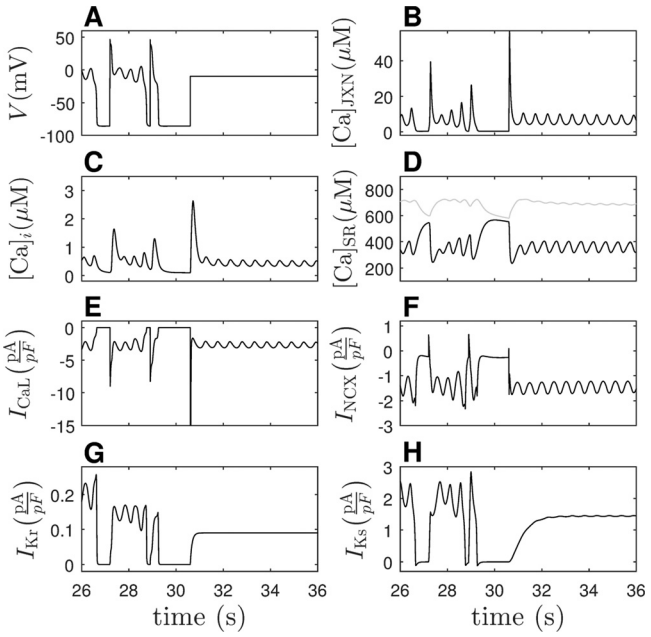

FIG. 5. Response to voltage clamping. The model simulation is identical to that from Fig. 3 until 30.6 s. At this point, once the next action potential is elicited, the voltage is clamped at the plateau value. Calcium oscillations persist under these conditions indicating that spontaneous systolic release of Ca^{2+} is not dependent on the L-type calcium channels. (a) Membrane voltage. (b), (c), and (d) Concentration of Ca^{2+} in JXN, cytoplasm, and SR, respectively. (e) Calcium dependent inactivation causes oscillations in I_{CaL}. Ca^{2+} concentrations continue to oscillate even when I_{CaL} is held constant (simulations not shown). (f), (g), and (h) Time course of I_{NCX}, I_{Kr}, and I_{Ks}. Here, the magnitude of I_{Kr} decreases until 30 s due to imposed block.

currents and Ca^{2+} concentration in the promotion of arrhythmias. When RyR2s were forced to closed states after 43.8 s of running the model at 800 ms cycle length (CL) (by which time EADs have fully developed), it resulted in the immediate disappearance of EADs and significant APD shortening. This occurred despite the fact that the amplitude of I_{CaL} initially increased because of much lower Ca^{2+} concentration in the JXN space and a decrease in Ca^{2+}-mediated I_{CaL} inhibition. The APD shortening and EAD elimination appeared to be caused by the elimination of the late increase in the inward I_{NCX} current, which—in the absence of RyR2 clamping—is related to the gradual Ca^{2+} re-accumulation in the JSR, consequent to secondary RyR2 opening and increase in Ca^{2+} in JXN and SL compartments (Fig. 6).

The essential role of NCX in EAD generation is confirmed by forcing I_{NCX} to zero after 44.1 s of model run, and leaving other model variables (including RyR2 opening) intact. This abolished EADs (Fig. 7). When I_{NCX} is set to zero, the secondary Ca^{2+} release from overloaded JSR is modified (due to slower Ca^{2+} removal from the JXN space), but not eliminated [Figs. 7(b) and 7(d)]. Nevertheless, the APD is dramatically shortened and no EADs occur, consistent with NCX requirement for Ca^{2+}-induced membrane depolarizations. I_{CaL} also plays an indispensable role in EAD generation, not just because it is required to replenish SR Ca^{2+} by letting Ca^{2+} into the cell but also to maintain adequate Ca^{2+} concentration in the JXN space. When I_{CaL} is forced to zero after 44.1 s of model run results is the premature termination of SR Ca^{2+} release by decreasing the Ca^{2+} concentration in the JXN space and closing the g1 gate of RyR2 (Fig. 8).

The behavior of this model was investigated under low extracellular potassium conditions (i.e., hypokalemia). Figure 9 show the results from a simulation with parameters identical to those from Fig. 3, except with linearly decreasing extracellular $[K^+]$ and a slightly different profile for I_{Kr} block [Fig. 9(b)]. EADs form due to I_{Kr} block at approximately 18 s and quickly result in salvos of EADs due to the low potassium concentration. During EAD salvos, I_{CaL} current [Fig. 9(h)] remains active, helping to maintain the elevated transmembrane voltage. Excess calcium from I_{CaL} is pumped to SR by SERCA, leading to intermittent opening of RyR2. Instantaneous RyR2 block is modeled at 30 s, by setting calcium release from SR to zero, and eliminates EADs immediately. In the absence of RyR2 block (or other intervention), EAD salvos persist indefinitely.

2-D model

In the 2-D model, we investigated the formation of both EADs and diastolic calcium release from SR, the latter causing Ca^{2+} waves and small DADs which are not arrhythmogenic but have been observed alongside EADs.[1] We did not find a combination of parameters for which the 0-D model

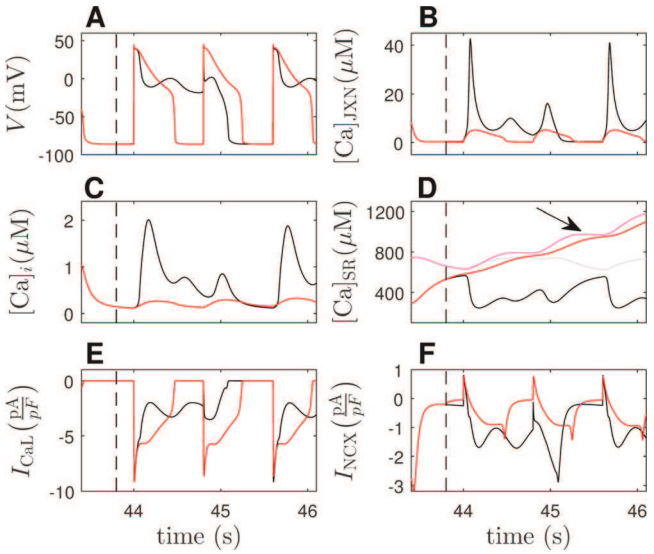

FIG. 6. Ca^{2+} release from JSR is required for EAD generation. The model is run at 800 ms pacing cycle length for 43.8 s with the time course of I_{Kr} block identical to that in Fig. 3, i.e., with a linear ramp down to 10%. After 43.8 s, Ca^{2+} release from the JSR is set to zero (denoted by a vertical dashed line in each panel) modeling instantaneous full block of RyR2, and the model evolution (red and pink lines) is compared with the model preserving the nominal JSR Ca^{2+} release (black and grey lines). (a) Membrane voltage. The EAD is eliminated and APD is substantially shortened with RyR2 block. (b) RyR2 block dramatically reduces Ca^{2+} concentration in the JXN compartment; the Ca^{2+} rise is caused essentially by the influx of Ca^{2+} via I_{CaL}. Note that without RyR2 block, Ca^{2} in the JXN space starts to rise again at about 44.5 s. This is primarily due to gradual rise of Ca^{2+} in the JSR [black tracing in panel (d)] and opening of RyR2 g2 gate. (c) RyR2 block eliminates the oscillation of Ca^{2+} in the cytoplasm. (d) JSR Ca^{2+} concentration is shown in red and black for modified and nominal conditions, respectively. NSR Ca^{2+} concentration is shown in pink and grey for modified and nominal conditions, respectively. Steady rise of Ca^{2+} concentration in SR (arrow) is caused by a combination of RyR2 block and ongoing SERCA activity. (e) I_{CaL} trace: here RyR2 block increases I_{CaL} during most of the shortened AP by decreasing its Ca^{2+}-dependent inactivation. (f) RyR2 block markedly attenuates the inward I_{NCX} current by decreasing the Ca^{2+} concentration in the JXN and SL compartments, which decreases the driving force for NCX. As shown below (Fig. 7), the inward I_{NCX} current in the absence of RyR2 block accounts for long APD.

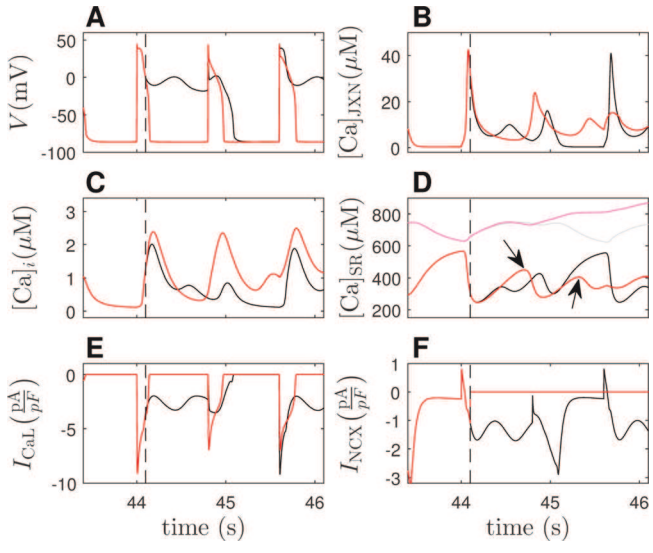

FIG. 7. Response to I_{NCX} block. Model parameters are similar to Fig. 6, but NCX is set to zero at 44.1 s (denoted by a vertical dashed line in each panel) just before the first EAD under nominal conditions instead of RyR2 Ca^{2+} release. Red (respectively black) lines show model behavior under modified (respectively nominal) conditions. (a) Membrane voltage. NCX block eliminates EADs and shortens APD. (b) NCX block modifies the secondary Ca^{2+} release from RyR2 and generally increases Ca^{2+} in JXN by removing one of the efflux mechanisms. (c) Ca^{2+} concentration in cytoplasm increases with NCX block. (d) JSR Ca^{2+} concentration is shown in red and black for modified and nominal conditions, respectively. NSR Ca^{2+} concentration is shown in pink and grey for modified and nominal conditions, respectively. Arrows highlight secondary Ca^{2+} release from JSR during diastole (i.e., when I_{CaL} is zero). (e) I_{CaL} elimination of the inward current provided by NCX shortens APD and duration of Ca^{2+} influx through L-type Ca^{2+} channels. (f) Time course of I_{NCX} in each simulation.

produced both EADs and diastolic calcium release from SR. However, by incorporating spatial heterogeneity in the 2-D model, a single model could display both behaviors. Panel (a) of Figs. 10 and 11 shows a schematic of such a model. In all compartments, the parameter $\mathbf{H_1}$, which describes the Hill coefficient of the g1 gate, was drawn from a normal distribution with mean of 4.2 and standard deviation of 1. For compartments in the upper-left hand corner, representing approximately 10% of the cell, the parameter $\mathbf{K_1}$ (the Ca^{2+} concentration in JXN producing half-maximum g1 opening) was chosen to be 0.05 mmol/l. In all other compartments, $\mathbf{K_1}$ was chosen randomly from a normal distribution with mean of 0.07 and standard deviation of 0.01 mmol/l. Smaller values of K1 require smaller concentrations of CA^{2+} in JXN to open g1, which increases the likelihood of DAD formation. Compartments in the upper-left corner had an SR calcium leak from parallel to g1 of $\mathbf{B} = 0.03$, all others used $\mathbf{B} = 0.01$; higher values of $\mathbf{B}$ tend to produce DADs while lower values result in EADS in the 0-D model. With these parameters, compartments in the upper-left corner more readily produced diastolic Ca^{2+}-release due to a lower threshold required for Ca^{2+}-induced Ca^{2+}-release from RyR2. In 2-D simulations, the onset of I_{Kr} block was also implemented with the same protocol used in simulations from Fig. 3. Note that relative to the original parameters from Ref. 26, the rate of diffusive coupling from JXN to SL and from SL to cytoplasm was increased to facilitate the propagation of diastolic calcium waves.

Using this model, we observe diastolic calcium release resulting in DADs after the cessation of fast pacing [see Figs. 10(b)–10(f)]. Upon the cessation of pacing, SR calcium is overloaded, leaking into the junctional space and ultimately causing a large calcium-induced calcium release. Calcium diffuses to adjacent compartments, first to the SL and then to JXN spaces, triggering a diastolic calcium wave. This wave traverses the length of the cell at a relatively constant speed, as shown by the pseudo-line scan in panel (b) of Fig. 10 (see animation 1 of supplementary material). Panels (c)–(e) show time courses of calcium concentrations and panel (f) shows transmembrane voltage illustrating the diastolic rise in calcium which leads to a DAD. Note that in simulations, I_{Kr} block is not required to produce DADs, but does facilitate their development by increasing the calcium concentrations in SR.

Figure 11 shows the same model from Fig. 10, paced at two different rates. Under relatively slow pacing at a rate of 1350 ms [panels (b)–(d)], we observe EADs stemming from secondary calcium release from SR. The calcium concentrations at spatially distinct locations throughout the cell are

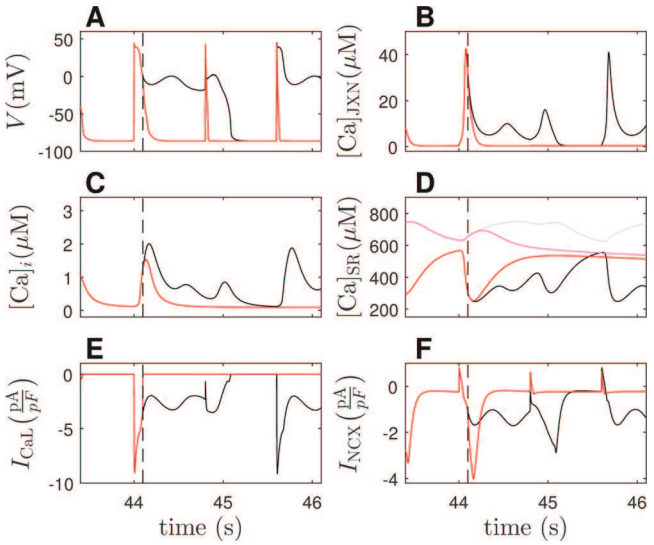

FIG. 8. Response to I_{CaL} block. Model parameters are similar to Figs. 6 and 7, but I_{CaL} is set to 0 at 44.1 s (denoted by a vertical dashed line in each panel) instead of RyR2 or NCX. Red (respectively black) lines show model behavior under modified (respectively nominal) conditions. (a) Membrane voltage. I_{CaL} elimination leads to premature termination of the AP starting at 44.1 s and collapse of APs starting at 44.8 s and later. (b) I_{CaL} termination decreases Ca^{2+} influx to JXN space. Decreased Ca^{2+} concentration in this compartment leads to RyR2 closure, subsequent elimination of SR Ca^{2+}-release, and monotonic decline in cytoplasmic Ca^{2+} (c). (d) JSR Ca^{2+} concentration is shown in red and black for modified and nominal conditions, respectively. NSR Ca^{2+} concentration is shown in pink and grey for modified and nominal conditions, respectively. Elimination of I_{CaL} reduces calcium influx to the cell, precipitating a gradual decline of Ca^{2+} in both JSR and NSR due to leak from SR. (e) Time course of I_{CaL} in each simulation. (f) Once SR Ca^{2+}-release is eliminated and cytoplasmic Ca^{2+} concentrations have declined, the I_{NCX} current is nearly eliminated.

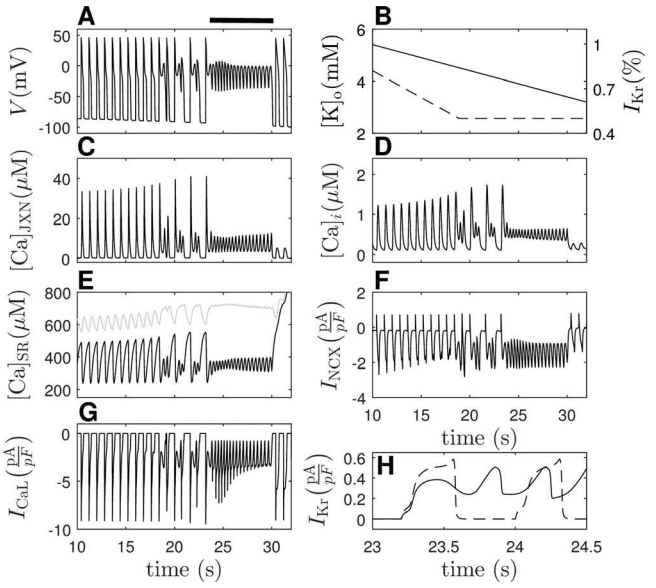

FIG. 9. Model response to low extracellular $[K^+]$. Extracellular potassium is decreases monotonically. Block of RyR2 is modeled instantaneously at 30 s, eliminating release from JSR. (a) Membrane voltage. The first EADs form at approximately 18 s due to I_{Kr} block. Hypokalemia results in subsequent EAD salvos, highlighted by the thick black line. Instantaneous RyR2 block at 30 s immediately terminates EADs. (b) The black line shows the extracellular potassium concentration gradually reduced from its nominal value which induces EAD salvos at approximately 23 s. The dashed line gives the time course of I_{Kr} block. (c) and (d) Junctional and cytoplasmic Ca^{2+} concentrations, respectively. (e) The black line (respectively grey line) shows the JSR (respectively NSR) Ca^{2+} concentration. (f) During EAD salvos, I_{NCX} remains active, facilitating the maintenance of elevated transmembrane voltage. (g) During EAD salvos, I_{CaL} remains active, helping maintain the elevated transmembrane voltage. Ca^{2+} influx from I_{CaL} is pumped to SR by SERCA, replenishing the Ca^{2+} concentration after each opening of RyR2. (h) The solid line shows a close-up of the I_{Kr} current at the initiation of an EAD salvo. The dashed line gives a comparison from a simulation which is identical except that the potassium concentration is at its nominal value. The reduction in I_{Kr} prolongs the AP plateau, contributing to the genesis of salvos of EADs.

cell synchronous, rising and falling in unison during the EADs (see animation 2 of supplementary material). As pacing becomes faster [panels (e)–(g)], EADs subside.

Under certain conditions, multifocal diastolic Ca^{2+} release was observed in 2-D simulations. For example, in Fig. 12, we choose the parameters for each compartment such that $\mathbf{K_1} = 0.005$ mmol/l, $\mathbf{B} = 0.05$, and $\mathbf{H_1}$ taken from a normal distribution with a mean of 4.6 and a unit standard deviation. For this choice of parameters, compartments with lower values of $\mathbf{H_1}$ more readily release Ca^{2+} from the SR after the cessation of pacing at 400 ms. In these simulations, diastolic Ca^{2+} release tends to begin in locations for which $\mathbf{H_1}$ is lower on average. In panel (a), three prominent foci are seen, denoted by arrows. As time progresses in panels (b) and (c), Ca^{2+} waves emanate from these foci, eventually enveloping the entire cell. Panel (d) shows a pseudo-line scan of Ca^{2+} in the SL space, for compartments along longitudinal midline (i.e., at W/2) (see animation 3 of supplementary material).

DISCUSSION

Impairment of ventricular repolarization is an important cause of life-threatening cardiac arrhythmias and sudden cardiac death. The mechanistic steps linking the APD prolongation to EAD and arrhythmias remain disputed and incompletely understood. The prevailing theory[17–19,36] proposes that EADs are primarily caused by I_{CaL} window current and eventual I_{CaL} reactivation and is independent of I_{NCX} and SR Ca^{2+} release. This is supported by the experimental evidence that EADs can be suppressed by blocking I_{CaL}, as well as by the results of mathematical modeling.[37–39] On the other hand, different experiments suggest a crucial role for Ca^{2+} release from SR and consequent augmentation of the inward I_{NCX} current as the critical step in EAD generation.[20,21] Note that this interpretation does not mean that EAD genesis is independent of transmembrane voltage, but rather, that the mechanism of EAD generation may be different than previously thought. We have recorded simultaneous voltage and cytoplasmic calcium optical signals from an isolated heart model of LQTS which strongly suggest that secondary calcium release from SR precedes and causes EADs. Similar data have been obtained by others.[23,24] The proposed mechanism has been recently summarized in a qualitative manner,[40] but formal mathematical modeling has not been performed to the best of our knowledge.

Here, we report a modification of one of the major models of rabbit ventricular myocyte that replicates several of the new experimental findings from the optical mapping experiments described above and allows for direct exploration of the possible role of SR Ca release in EAD triggering. The

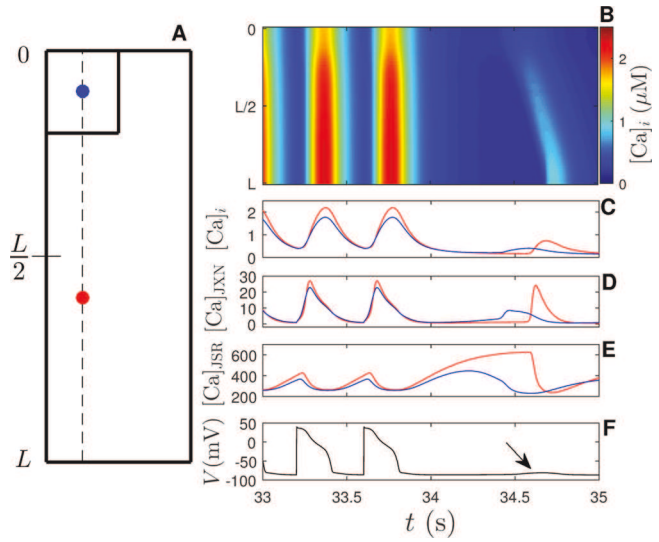

FIG. 10. Simulation with diastolic SR Ca^{2+}-release. (a) Schematic of a single cell with length L. In the top-left corner, parameters are chosen so that this region spontaneously initiates DAD-like Ca^{2+} release after the cessation of 400 ms pacing. (b) Pseudo-line scan of the Ca^{2+} concentration in the cytoplasmic compartment. This scan is taken along the dashed line from panel (a). Diastolic Ca^{2+} release occurs spontaneously upon cessation of pacing in the top-left portion of the cell, initiating a Ca^{2+} wave. (c)–(e) Blue and red curves correspond to cytoplasmic, JXN, and JSR Ca^{2+} concentrations, respectively. Colors correspond to values at dots of the same color in panel (a). (f) Membrane voltage. Diastolic SR Ca^{2+}-release activates I_{NCX}, triggering a DAD at approximately 34.6 s, denoted by the arrow.

main changes introduced into the SPB model were motivated by experimental results. First, the predominant localization of cardiac SERCA to NSR is well established,[41] justifying the division of the SR compartment into JSR and NSR subdivisions. It is reasonable to assume a Ca^{2+} concentration gradient between these compartments due to limited diffusion speed, although the precise value of Ca^{2+}

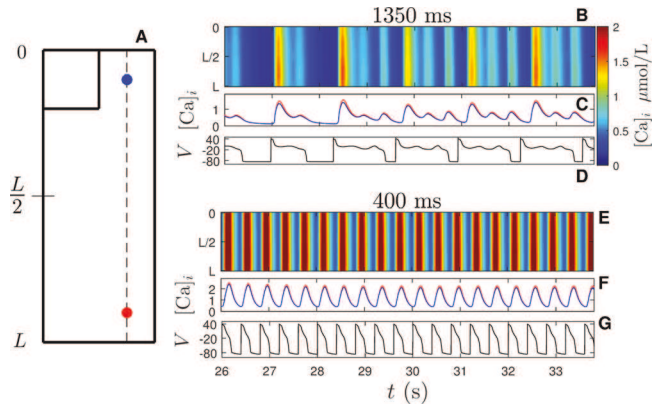

FIG. 11. 2-D model simulation at two different pacing rates. (a) Schematic of the 2-D model with length L. Relative to the other compartments, SR Ca^{2+} leak is larger and the threshold for opening RyR2 is decreased in the region in the top-left corner. Model parameters are identical to those from Fig. 10. (b)-(d) and (e)-(g) show simulations with the cell paced at 1350 and 400 ms, respectively. Panels (b) and (e) show Pseudo-line scan of Ca^{2+} concentration in the cytoplasmic compartment. The scan is taken along the dashed line from panel (a). Panels (c) and (f) show cytoplasmic Ca^{2+} at spatial locations corresponding dots of identical color from panel (a). Panels (d) and (g) show the transmembrane voltage during simulations. Pacing at 1350 ms results in EADs with cell synchronous Ca^{2+} behavior. Faster pacing eliminates EADs.

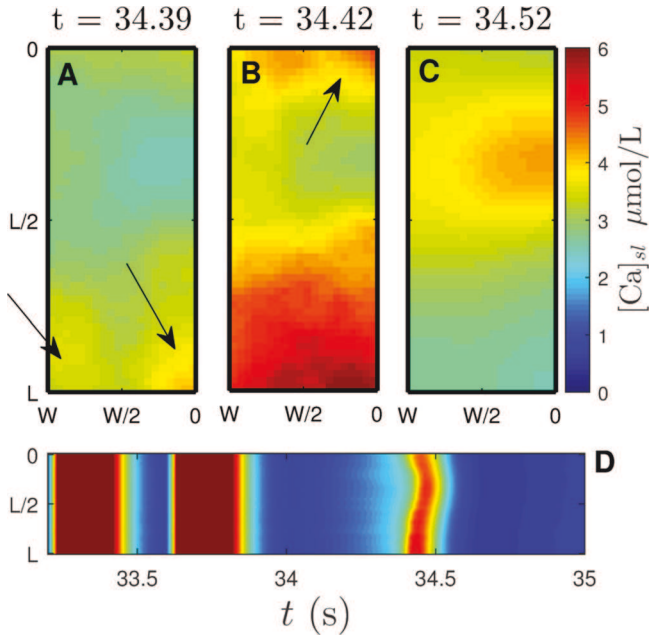

FIG. 12. Multifocal Ca^{2+} release. Panels (a)-(c) show snapshots of Ca^{2+} in the SL compartments after pacing at 400 ms is stopped. Diastolic Ca^{2+}-release from SR is initiated at three foci, highlighted with black arrows in panel (a). As Ca^{2+} diffuses from high to low concentration, it initiates Ca^{2+} release in adjacent compartments, shown in panels (b) and (c). Panel (d) shows a pseudo-line scan along the midline (i.e., at W/2).

diffusion coefficient in SR is disputed.[28,42] Abundant data are available on the activation of RyR2 by increase in JSR Ca^{2+} concentration[29–31] and its inactivation by prolonged Ca^{2+} elevation in the dyadic space.[43,44] These 2 processes are conceptualized separately in this model as g2 and g3 gates, with the g1 gate accounting for the CICR.

The 0-D model replicates the gradual appearance of ectopic activity during gradual onset of I_{Kr} block, with initially monophasic AP followed by APs with single EAD, and eventual development double and multiple EADs. The model also reproduces the secondary systolic elevations of Ca^{2+} transient related to EADs in optical mapping experiments (cf. Fig. 2 in Ref. 22). The role of individual ion channels and pumps in the EAD generation can be explored in the model by forcing instantaneous changes of individual currents without direct effect on the others, something that is difficult to accomplish experimentally *in vivo*. The *in silico* experiments reported here show that the secondary Ca^{2+} release from JSR, related primarily to JSR Ca^{2+} overload, is the main mechanism underlying EADs, by means of activation of the electrogenic NCX exchanger: elimination of either the secondary Ca^{2+} release or of the NCX activity results in immediate disappearance of EADs while Ca^{2+} oscillations persist when the voltage is clamped at its plateau. This is consistent with the reports that both inhibition of intracellular Ca^{2+} cycling by ryanodine and thapsigargin (blockers of the RyR2 and SERCA, respectively), and pharmacological block of NCX eliminates TdP in isolated hearts.[22,45]

Increasing the pacing rate of the model suppresses both Ca^{2+} oscillations and EADs, a finding consistent with both clinical experience and experimental results. In the model,

shortening the CL leads to the onset of the next AP and to JSR emptying through the normal CICR mechanism before the JSR is replenished by Ca^{2+} diffusion from NSR to a degree which would cause the secondary Ca^{2+} release. The model also produces the facilitation of salvos of EADs in hypokalemia conditions.

Pinpointing the exact mechanisms of arrhythmia in the long QT syndrome is still an open problem, but most AP clamp studies support the hypothesis that abnormal Ca^{2+} dynamics are required to elicit EADs. In an attempt to resolve this issue, tests have been conducted on conditions that produce EADs in isolated myocytes and trying to block or promote SR Ca^{2+} release (RyR2 blockade, SR Ca^{2+} depletion, or chelation of cytosolic Ca^{2+}) or by controlling the membrane potential during the AP plateau (AP clamp, suppression of I_{NCX}). For example, EADs and intracellular Ca^{2+} waves were elicited by H_2O_2 (oxidative stress) or by isoproterenol (increase in the Ca^{2+} load) plus Bay K 8644 (L-type Ca^{2+} channel agonist).[46] The suppression of EADs during an AP clamp eliminated Ca^{2+} waves by H_2O_2 but not by isoproterenol plus Bay K 8644 suggesting voltage control in the first but not the second condition.[46] However, the multiple targets of H_2O_2 and prior findings that BayK 8644 alone can elicit EADs[17] complicate the interpretation of these experiments. In myocytes with hyper-reactive (or leaky) RyR2, spontaneous SR Ca^{2+} release was shown to elicit EADs; that is, Ca^{2+} elevation altered the voltage in myocytes isolated from models of CPVT,[10] heart failure,[13] and congenital LQT2 rabbits.[47] In myocytes treated with ATXIII (I_{Na} agonist) to mimic aLQT type 3, spontaneous SR Ca^{2+} release elicited EADs which were suppressed when Ca^{2+} waves were eliminated with the high-affinity Ca^{2+} chelator BAPTA.[48] More work is necessary to definitively pinpoint the precise set of steps which give rise to EADs in the intact heart, but the model presented here is consistent with the hypothesis that EADs are driven by abnormal calcium release due to overloaded Ca^{2+} in SR.

Simulations of the AP and Ca^{2+} transients (CaT) have thus far failed to accurately reproduce the amplitude and time-course of experimental measurements at various heart rates, with worse outcomes at slow rates.[26] A major challenge has been the complex properties of RyR2 in the face of dynamic cytosolic and luminal Ca^{2+} levels. Based on experimentally derived relationship between the amount of SR Ca^{2+} release and SR Ca^{2+} load, Shiferaw *et al.*, inserted a nonlinear release-to-load relationship in a model that successfully reproduced CaT alternans but did so, only in the presence of diastolic Ca^{2+} alternans in the SR lumen.[49] However, experimental evidence showed that CaT alternans can occur in the absence of diastolic luminal SR Ca^{2+} alternans[50] and the steep release-load relationship at high luminal SR Ca^{2+} remained *ad hoc*. Instead of a nonlinear release-load relationship, Restrepo *et al*. modeled RyR2 gating based on its interaction with the Ca^{2+} buffering properties of calsequestrin in the SR.[51] The latter stochastic Markov model of RyR2 could predict cytosolic CaT alternans in the absence of diastolic luminal Ca^{2+} alternans in rodent APs at high heart rates. The same model was used to show that Ca^{2+} elevation preceded EADs and EADs were elicited by spontaneous SR Ca^{2+} release.[52] The current model based on 3 RyR2 gates is unique in its ability to predict APs and CaTs during a bradycardia and that robust EADs are elicited by synchronous secondary Ca^{2+} elevations during systole.

We have developed a 2-D version of the model to explore the spatio-temporal features of intracellular Ca^{2+} dynamics. We find that the secondary systolic Ca^{2+} peak occurs across the cell in an approximately cell-synchronous manner, even when a degree of spatial heterogeneity is introduced into the RyR2 kinetics. This resembles the results of subcellular optical mapping experiments.[1] The same spatial heterogeneity generates a propagated Ca^{2+} wave in diastole after cessation of rapid pacing of the 2-D model, a well-known phenomenon reported in tissue and isolated cells on multiple occasions.[53,54] A modification of the model parameters gives rise to multifocal intracellular Ca^{2+} dynamics which we have occasionally observed in tissue experiments under LQTS conditions.

Limitations/future direction

Although the model replicates several recently observed features of Ca^{2+} dynamics during repolarization delay, in several respects, it remains inadequate and perhaps naıve. For one, some established and quantitatively important features of intracellular Ca^{2+} handling are not addressed—e.g., the role of Ca^{2+} buffering in mitochondrial matrix.[55,56] Second, the modeled cell behavior differs from the experimental observations in some important details. For example, we have always observed that the appearance of systolic Ca^{2+} oscillations precedes the appearance of EAD in the perfused heart experiments, but in the model, they were always immediately accompanied by EADs. Also, in the heart experiments, the upstroke of Ca^{2+} release always precedes the upstroke of EADs by tens of milliseconds at least, but in the model, the EAD upstroke occurs nearly simultaneously, although the model manipulation described in the Results section clearly shows that the Ca^{2+} release causes EAD in the model. It is unclear whether this is best explained by the presence of millions of connected cells in the perfused heart experiments, which are well coupled electrically but poorly with respect to intercellular Ca^{2+} diffusion, or whether the model fails to replicate real single-cell behavior due to the lack of systematic exploration of the parameter space or other reasons. We have not attempted to model tissue composed of coupled cells with heterogeneous Ca^{2+} dynamics, though this would certainly be important for understanding of the heart behavior.

These and other issues may be explored with future modifications of the model. Nevertheless, we feel that the model does provide new insights into the role of Ca^{2+} handling in arrhythmogenesis during repolarization delay.

SUPPLEMENTARY MATERIAL

See supplementary material for animations of Figures 10, 11, and 12 to help visualize the simulations of Ca^{2+} dynamics under various conditions which closely track experimental data.[1,7] The supplementary material contains legends for animations 1, 2, and 3 followed by detailed

changes made to the SPB model. Animation 1: Diastolic Ca^{2+} waves postpacing—Animated version of simulations from Fig. 10. The cell is paced with a period of 400 ms until t = 33.6 s. The top panel shows the cytosolic Ca^{2+} concentration. After cessation of pacing, a diastolic calcium wave begins at the lower-right hand corner and traverses the length of the cell. Transmembrane voltage is shown in the middle panel, with an EAD occurring at approximately 34.7 s. The bottom panel shows the cytosolic Ca^{2+} at locations corresponding to the white dots in the top panel. Vertical black bars denote the time progression. Animation 2: Synchronous Ca^{2+} dynamics—Animated version of the 1350 ms paced simulations from Fig. 11. The top panel shows the cytosolic Ca^{2+} concentration. Transmembrane voltage is shown in the middle panel. The bottom panel shows the cytosolic Ca^{2+} at locations corresponding to the white dots in the top panel. Vertical black bars denote the time progression. While the magnitude of cytosolic Ca^{2+} is spatially heterogeneous, the dynamics are cell synchronous, rising, and falling in unison. Animation 3: Multifocal diastolic Ca^{2+} release—Animated version of simulations from Fig. 12. The cell is paced with a period of 400 ms until t = 33.6 s. The top panel shows the cytosolic Ca^{2+} concentration. Transmembrane voltage is shown in the middle panel. The bottom panel shows the cytosolic Ca^{2+} at locations corresponding to the white dots in the top panel. Vertical black bars denote the time progression. Diastolic calcium waves begin at locations for which $\mathbf{H_1}$ is relatively low.

ACKNOWLEDGMENTS

The authors are indebted to Dr. J. Puglisi, who has kindly provided the updated code for the original SPB model. This work was supported by Bridge Funds from the School of Medicine to G.S. and by National Science Foundation Grant No. NSF-1602841 to D.W. Dedicated to the Memory of our dearest friend and colleague Dr. Jan Němec.

APPENDIX: MODEL EQUATIONS AND PARAMETERS

The changes made to the original SPB model[25] are summarized below.

1. Reformulation of sarcoplasmic reticulum compartments

The single SR compartment of the SPB model is replaced by 2 compartments (junctional SR (JSR) and non-junctional SR (NSR)) of the same volume (cell volume of 0.035) and same Ca^{2+} buffering properties. These 2 compartments are diffusionally coupled with respect to free Ca^{2+} concentration, with the strength of coupling 0.06/ms unless stated otherwise. The transport of Ca^{2+} from the cytoplasm to SR via SERCA occurs solely into the NSR compartment, and Ca^{2+} release from SR into the dyadic space through RyR2 occurs solely from the JSR compartment. The Ca^{2+} transport via plasma membrane Ca^{2+} pump and cytoplasmic dye buffering have been eliminated in the modified model.

2. Reformulation of ryanodine receptor

The RyR2 is now modeled with 3 serial gates governed by HH formalism as detailed in the Methods section. Specifically, the equation describing Ca current in the SPB model, i.e.,

$$J_{SRCaRel} = k_s . O . \left([Ca]_{SR} - [Ca]_{jct}\right)$$

[Eq. (106) from Ref. 25] is replaced by

$$J_{SRCaRel} = k_{\max} . (B + O_1) . O_2 . O_3 . \left([Ca]_{JSR} - [Ca]_{jct}\right),$$

where O_1, O_2, and O_3 are the open probabilities of the gates g1, g2, and g3, respectively. The B parameter describes the relative strength of the passive Ca^{2+} leak in parallel to the g1 gate. The original SPB model had the SR Ca^{2+} leak modeled by Eq. (107)—this has been eliminated in the new model.

The variables O_1, O_2, and O_3 are described by the following equations:

$$\frac{dO_1}{dt} = \frac{(ssO_1 - O_1)}{\tau_1},$$
$$\frac{dO_2}{dt} = \frac{(ssO_2 - O_2)}{\tau_2},$$
$$\frac{dO_3}{dt} = \frac{(ssO_3 - O_3)}{\tau_3},$$

where ssO_1 and τ_1 denote the steady-state and time-constant of the g1 gate, etc.

The steady-state open probabilities are described by

$$ssO_1 = \frac{\left(\frac{[Ca]_{jct}}{K_1}\right)^{H_1}}{1 + \left(\frac{[Ca]_{jct}}{K_1}\right)^{H_1}},$$
$$ssO_2 = \frac{\left(\frac{[Ca]_{JSR}}{K_2}\right)^{H_2}}{1 + \left(\frac{[Ca]_{JSR}}{K_2}\right)^{H_2}},$$
$$ssO_3 = \frac{1}{1 + \left(\frac{[Ca]_{jct}}{K_3}\right)^{H_3}}.$$

The parameters K_1, K_2, K_3, H_1, H_2, and H_3 are constant in the model and are listed in Table I. The same is true of the time constants τ_1 and τ_3. The time-constant τ_2 depends on the Ca^{2+} concentration in JSR (slower kinetics when Ca^{2+} is low)

$$\tau_2 = \tau_0 . \left(1 + \frac{1}{\left(\frac{[Ca]_{JSR}}{K_4}\right)^{H_4}}\right),$$

where the parameters τ_0, K_4, and H_4 are constant and listed in Table I.

TABLE I. List of parameters in the SPB model and changes implemented in the current model.

Parameter	Parameter description	Value in SPB	Value in modified model	Unit
K_1	Half-maximum Ca concentration of g1	—	0.01	mmol/l
K_2	Half-maximum Ca concentration of g2	—	0.35	mmol/l
K_3	Half-maximum Ca concentration of g3	—	0.005	mmol/l
K_4	Involved in τ_2 calculation	—	1.0	mmol/l
H_1	Hill coefficient of g1	—	2.7	1
H_2	Hill coefficient of g2	—	3.5	1
H_3	Hill coefficient of g3	—	2	1
H_4	Involved in τ_2 calculation	—	4	1
τ_0	Involved in τ_2 calculation	—	0.02	ms
τ_1	Time-constant of g1	—	20	ms
τ_3	Time-constant of g3	—	300	ms
B	Ca leak parallel to g1 gate	—	0.004	1
k_{max}	Maximal SR release rate constant (all gates or RyRs open)	—	0.2	ms^{-1}
Fx_{CaL} junction	Fraction of L-type channels localized to junctional membrane	0.9	0.5	1
$\bar{I}_{NaK}$	Na/K ATPase current density	1.91	1.90719	A/F
$\bar{I}_{NCX}$	NCX current density	9	5	A/F
Na B_{max} junction	Na buffering capacity in junctional space	3.7	7.561	mmol/l
Csqn B_{max}	Calsequestrin Ca buffering capacity	0.14	0.28	mmol/l
SLhigh SL B_{max}	Ca buffering capacity, high affinity, SL space	0.0134	0.005	mmol/l
gkr at $K_o = 5.4$ mmol/l	Maximal I_{Kr} current conductance at $K_o = 5.4$ mmol/l	0.03	0.045	mS/μF
$\bar{G}_{Ks}$	Maximal I_{Ks} current conductance	$0.07\left(0.057+\frac{0.19}{1+\exp\left(-7.2+\left(\frac{pCa}{0.6}\right)\right)}\right)$ i.e. the original Eq. (50)	$0.82\left(0.057+\frac{0.19}{1+\exp(-7.2+(pCa/0.6))}\right)$	mS/μF
$Gt_{o,s}$	Maximal I_{to} current conductance, slow component	0.02	0.06	mS/μF
$G_{to,f}$	Maximal I_{to} current conductance, fast component	0.06	0.02	mS/μF
P_{Ca}	Related to L-type channel permeability to Ca^{2+} ions	0.00054	0.001188	cm/s
J_ca_juncsl	Diffusional coupling for Ca^{2+} ions, JXN to SL	9.8728×10^{-14}	2.4724×10^{-12}	l/ms
J_ca_slmyo	Diffusional coupling for Ca^{2+} ions, SL to cytoplasm	3.5244×10^{-12}	7.4485×10^{-13}	l/ms

3. Other changes

The changes of parameter values with respect to the SPB model are listed in Table I. Among other changes, the conductance of I_{Ks} and I_{CaL} was increased to simulate isoproterenol effect, and the Ca^{2+} diffusion coupling between compartments was modified.

The description of ICaL activation and inactivation gates has been shifted slightly, so that the original model equations (78)–(81) in Ref. 25 are replaced with

$$\frac{df_{CaB}}{dt} = 1.7\,[Ca]_C\,(1-f_{CaB}) - 0.012 f_{CaB},$$

$$d_\infty = \frac{1}{1+\exp\left(-\frac{V+23.5}{6.0}\right)},$$

$$\tau_d = d_\infty \frac{1-\exp\left(-\frac{V+23.5}{6.0}\right)}{0.035\,(V+23.5)},$$

$$f_\infty = \frac{1}{1+\exp\left((V+42)/3.6\right)} + \frac{1}{1+\exp\left((45-V)/20\right)}.$$

The plateau K^+ current introduced into a later version of the SPB model by the authors has been retained. It is formulated as

$$I_{Kp} = \frac{0.001}{1+\exp\left((7.488-V)/5.98\right)}\cdot(V-E_K).$$

The slow component of the Ito has been modified by the authors of the original model in a later version in such a way that the R_s gating variable now achieves the steady state with a finite time constant. This modification has been retained. Specifically, Eq. (63) of the original model now becomes

$$I_{to,s} = G_{to,s}\cdot X_{to,s}\cdot\left(Y_{to,s}+0.5.R_s\right)(V-E_K),$$

where the steady-state value of R_s is described by the original Eq. (60), and the time constant in ms is defined as

$$\tau_{Rto,s} = \frac{2800}{1+\exp\left((V+60)/10\right)} + 220.$$

[1]J. J. Kim, J. Němec, Q. Li, and G. Salama, "Synchronous systolic subcellular Ca^{2+}-elevations underlie ventricular arrhythmia in drug-induced long QT type 2," Circ.: Arrhythmia Electrophysiol. **8**, 703–712 (2015).
[2]D. M. Bers, "Cardiac excitation-contraction coupling," Nature **415**, 198–205 (2002).
[3]F. Fabiato and A. Fabiato, "Excitation-contraction coupling and regulation of contractility studied on isolated adult myocardial cells," Acta Cardiol. **27**, 243–248 (1972).
[4]F. Fabiato, A. Fabiato, and E. H. Sonnenblick, "Isolated myocardial cells of adult mammals. Analytical study of contractility and of excitation-contraction coupling," J. Physiol. (Paris) **63**, 210A (1971).
[5]B. R. Choi and G. Salama, "Simultaneous maps of optical action potentials and calcium transients in guinea-pig hearts: Mechanisms underlying concordant alternans," J. Physiol. **529**(Pt 1), 171–188 (2000).
[6]B. R. Choi, W. Jang, and G. Salama, "Spatially discordant voltage alternans cause wavebreaks in ventricular fibrillation," Heart Rhythm **4**, 1057–1068 (2007).

[7]J. J. Kim, J. Němec, R. Papp, R. Strongin, J. J. Abramson, and G. Salama, "Bradycardia alters Ca(2+) dynamics enhancing dispersion of repolarization and arrhythmia risk," Am. J. Physiol. Heart Circ. Physiol. **304**, H848–H860 (2013).

[8]D. Terentyev, A. Nori, M. Santoro, S. Viatchenko-Karpinski, Z. Kubalova, I. Gyorke *et al.*, "Abnormal interactions of calsequestrin with the ryanodine receptor calcium release channel complex linked to exercise-induced sudden cardiac death," Circ. Res. **98**, 1151–1158 (2006).

[9]M. Cerrone, C. Napolitano, and S. G. Priori, "Catecholaminergic polymorphic ventricular tachycardia: A paradigm to understand mechanisms of arrhythmias associated to impaired Ca(2+) regulation," Heart Rhythm **6**, 1652–1659 (2009).

[10]B. C. Knollmann, N. Chopra, T. Hlaing, B. Akin, T. Yang, K. Ettensohn *et al.*, "Casq2 deletion causes sarcoplasmic reticulum volume increase, premature Ca^{2+} release, and catecholaminergic polymorphic ventricular tachycardia," J. Clin. Invest. **116**, 2510–2520 (2006).

[11]J. R. Berlin, M. B. Cannell, and W. J. Lederer, "Cellular origins of the transient inward current in cardiac myocytes. Role of fluctuations and waves of elevated intracellular calcium," Circ. Res. **65**, 115–126 (1989).

[12]M. R. Rosen, "Cellular electrophysiology of digitalis toxicity," J. Am. Coll. Cardiol. **5**, 22A–34A (1985).

[13]A. E. Belevych, D. Terentyev, R. Terentyeva, Y. Nishijima, A. Sridhar, R. L. Hamlin *et al.*, "The relationship between arrhythmogenesis and impaired contractility in heart failure: Role of altered ryanodine receptor function," Cardiovasc. Res. **90**, 493–502 (2011).

[14]D. M. Roden, "Clinical practice: Long-QT syndrome," N. Engl. J. Med. **358**, 169–176 (2008).

[15]L. X. Cubeddu, "Drug-induced inhibition and trafficking disruption of ion channels: Pathogenesis of QT abnormalities and drug-induced fatal arrhythmias," Curr. Cardiol. Rev. **12**, 141–154 (2016).

[16]B. Surawicz, "Electrophysiologic substrate of torsades de pointes: Dispersion of repolarization or early afterdepolarizations?," J. Am. Coll. Cardiol. **14**, 172–184 (1989).

[17]C. T. January and J. M. Riddle, "Early afterdepolarizations: Mechanism of induction and block. A role for L-type Ca^{2+} current," Circ. Res. **64**, 977–990 (1989).

[18]E. Marban, S. W. Robinson, and W. G. Wier, "Mechanisms of arrhythmogenic delayed and early afterdepolarizations in ferret ventricular muscle," J. Clin. Invest. **78**, 1185–1192 (1986).

[19]C. H. Luo and Y. Rudy, "A dynamic model of the cardiac ventricular action potential. II. Afterdepolarizations, triggered activity, and potentiation," Circ. Res. **74**, 1097–1113 (1994).

[20]P. G. Volders, M. A. Vos, B. Szabo, K. R. Sipido, S. H. de Groot, A. P. Gorgels *et al.*, "Progress in the understanding of cardiac early afterdepolarizations and torsades de pointes: Time to revise current concepts," Cardiovasc. Res. **46**, 376–392 (2000).

[21]B. R. Choi, F. Burton, and G. Salama, "Cytosolic Ca^{2+} triggers early afterdepolarizations and Torsade de pointes in rabbit hearts with type 2 long QT syndrome," J. Physiol. **543**, 615–631 (2002).

[22]J. Němec, J. J. Kim, B. Gabris, and G. Salama, "Calcium oscillations and T-wave lability precede ventricular arrhythmias in acquired long QT type 2," Heart Rhythm **7**, 1686–1694 (2010).

[23]M. Maruyama, S. F. Lin, Y. Xie, S. K. Chua, B. Joung, S. Han *et al.*, "Genesis of phase 3 early afterdepolarizations and triggered activity in acquired long-QT syndrome," Circ.: Arrhythmia Electrophysiol. **4**, 103–111 (2011).

[24]P. C. Chang, H. T. Wo, H. L. Lee, S. F. Lin, M. S. Wen, Y. Chu *et al.*, "Role of sarcoplasmic reticulum calcium in development of secondary calcium rise and early afterdepolarizations in long QT syndrome rabbit model," PLoS One **10**, e0123868 (2015).

[25]T. R. Shannon, F. Wang, J. Puglisi, C. Weber, and D. M. Bers, "A mathematical treatment of integrated Ca dynamics within the ventricular myocyte," Biophys. J. **87**, 3351–3371 (2004).

[26]A. Parikh, R. Mantravadi, D. Kozhevnikov, M. A. Roche, Y. Ye, L. J. Owen *et al.*, "Ranolazine stabilizes cardiac ryanodine receptors: A novel mechanism for the suppression of early afterdepolarization and torsades de pointes in long QT type 2," Heart Rhythm **9**, 953–960 (2012).

[27]D. X. Brochet, D. Yang, A. Di Maio, W. J. Lederer, C. Franzini-Armstrong, and H. Cheng, "Ca^{2+} blinks: Rapid nanoscopic store calcium signaling," Proc. Natl. Acad. Sci. U.S.A. **102**, 3099–3104 (2005).

[28]E. Picht, A. V. Zima, T. R. Shannon, A. M. Duncan, L. A. Blatter, and D. M. Bers, "Dynamic calcium movement inside cardiac sarcoplasmic reticulum during release," Circ. Res. **108**, 847–856 (2011).

[29]W. Chen, R. Wang, B. Chen, X. Zhong, H. Kong, Y. Bai *et al.*, "The ryanodine receptor store-sensing gate controls Ca^{2+} waves and Ca^{2+}-triggered arrhythmias," Nat. Med. **20**, 184–192 (2014).

[30]D. Jiang, W. Chen, R. Wang, L. Zhang, and S. R. Chen, "Loss of luminal Ca^{2+} activation in the cardiac ryanodine receptor is associated with ventricular fibrillation and sudden death," Proc. Natl. Acad. Sci. U.S.A. **104**, 18309–18314 (2007).

[31]D. R. Laver, "Ca^{2+} stores regulate ryanodine receptor Ca^{2+} release channels via luminal and cytosolic Ca^{2+} sites," Biophys. J. **92**, 3541–3555 (2007).

[32]L. J. DeFelice and I. Aurora, "Chaotic states in a random world: Relationship between the nonlinear differential equations of excitability and the stochastic properties of ion channels," J. Stat. Phys. **70**, 339–354 (1993).

[33]D. Colquhoun and A. G. Hawkes, *The Principles of the Stochastic Interpretation of Ion-Channel Mechanisms* (Springer, New York, 2009).

[34]J. Nickolls, I. Buck, M. Garland, and K. Skadron, "Scalable parallel programming with CUDA," Queue **6**, 40–53 (2008).

[35]S. Rush and H. Larsen, "A practical algorithm for solving dynamic membrane equations," IEEE Trans. Biomed. Eng. **25**, 389–392 (1978).

[36]M. G. Chang, C. Y. Chang, E. de Lange, L. Xu, B. O'Rourke, H. S. Karagueuzian *et al.*, "Dynamics of early afterdepolarization-mediated triggered activity in cardiac monolayers," Biophys. J. **102**, 2706–2714 (2012).

[37]M. G. Chang, D. Sato, E. de Lange, J. H. Lee, H. S. Karagueuzian, A. Garfinkel *et al.*, "Bi-stable wave propagation and early afterdepolarization-mediated cardiac arrhythmias," Heart Rhythm **9**, 115–122 (2012).

[38]D. X. Tran, D. Sato, A. Yochelis, J. N. Weiss, A. Garfinkel, and Z. Qu, "Bifurcation and chaos in a model of cardiac early afterdepolarizations," Phys. Rev. Lett. **102**, 258103 (2009).

[39]P. C. Viswanathan and Y. Rudy, "Pause induced early afterdepolarizations in the long QT syndrome: A simulation study," Cardiovasc. Res. **42**, 530–542 (1999).

[40]J. Němec, J. J. Kim, and G. Salama, "The link between abnormal calcium handling and electrical instability in acquired long QT syndrome—Does calcium precipitate arrhythmic storms?," Prog. Biophys. Mol. Biol. **120**, 210–221 (2016).

[41]F. Swift, C. Franzini-Armstrong, L. Oyehaug, U. H. Enger, K. B. Andersson, G. Christensen *et al.*, "Extreme sarcoplasmic reticulum volume loss and compensatory T-tubule remodeling after Serca2 knockout," Proc. Natl. Acad. Sci. U.S.A. **109**, 3997–4001 (2012).

[42]P. Swietach, K. W. Spitzer, and R. D. Vaughan-Jones, "Ca^{2+}-mobility in the sarcoplasmic reticulum of ventricular myocytes is low," Biophys. J. **95**, 1412–1427 (2008).

[43]H. S. Hwang, F. R. Nitu, Y. Yang, K. Walweel, L. Pereira, C. N. Johnson *et al.*, "Divergent regulation of ryanodine receptor 2 calcium release channels by arrhythmogenic human calmodulin missense mutants," Circ. Res. **114**, 1114–1124 (2014).

[44]D. R. Laver, C. H. Kong, M. S. Imtiaz, and M. B. Cannell, "Termination of calcium-induced calcium release by induction decay: An emergent property of stochastic channel gating and molecular scale architecture," J. Mol. Cell Cardiol. **54**, 98–100 (2013).

[45]P. Milberg, C. Pott, M. Fink, G. Frommeyer, T. Matsuda, A. Baba *et al.*, "Inhibition of the Na^+/Ca^{2+} exchanger suppresses torsades de pointes in an intact heart model of long QT syndrome-2 and long QT syndrome-3," Heart Rhythm **5**, 1444–1452 (2008).

[46]Z. Zhao, H. Wen, N. Fefelova, C. Allen, A. Baba, T. Matsuda *et al.*, "Revisiting the ionic mechanisms of early afterdepolarizations in cardiomyocytes: Predominant by Ca waves or Ca currents?," Am. J. Physiol. Heart Circ. Physiol. **302**, H1636–H1644 (2012).

[47]D. Terentyev, C. M. Rees, W. Li, L. L. Cooper, H. K. Jindal, X. Peng *et al.*, "Hyperphosphorylation of RyRs underlies triggered activity in transgenic rabbit model of LQT2 syndrome," Circ. Res. **115**, 919–928 (2014).

[48]B. Horvath, T. Banyasz, Z. Jian, B. Hegyi, K. Kistamas, P. P. Nanasi *et al.*, "Dynamics of the late Na(+) current during cardiac action potential and its contribution to afterdepolarizations," J. Mol. Cell Cardiol. **64**, 59–68 (2013).

[49]Y. Shiferaw, M. A. Watanabe, A. Garfinkel, J. N. Weiss, and A. Karma, "Model of intracellular calcium cycling in ventricular myocytes," Biophys. J. **85**, 3666–3686 (2003).

[50]E. Picht, J. DeSantiago, L. A. Blatter, and D. M. Bers, "Cardiac alternans do not rely on diastolic sarcoplasmic reticulum calcium content fluctuations," Circ. Res. **99**, 740–748 (2006).
[51]J. G. Restrepo, J. N. Weiss, and A. Karma, "Calsequestrin-mediated mechanism for cellular calcium transient alternans," Biophys. J. **95**, 3767–3789 (2008).
[52]Z. Song, C. Y. Ko, M. Nivala, J. N. Weiss, and Z. Qu, "Calcium-voltage coupling in the genesis of early and delayed afterdepolarizations in cardiac myocytes," Biophys. J. **108**, 1908–1921 (2015).
[53]J. A. Wasserstrom, Y. Shiferaw, W. Chen, S. Ramakrishna, H. Patel, J. E. Kelly *et al.*, "Variability in timing of spontaneous calcium release in the intact rat heart is determined by the time course of sarcoplasmic reticulum calcium load," Circ. Res. **107**, 1117–1126 (2010).
[54]K. Fujiwara, H. Tanaka, H. Mani, T. Nakagami, and T. Takamatsu, "Burst emergence of intracellular Ca^{2+} waves evokes arrhythmogenic oscillatory depolarization via the Na^{+}-Ca^{2+} exchanger: Simultaneous confocal recording of membrane potential and intracellular Ca^{2+} in the heart," Circ. Res. **103**, 509–518 (2008).
[55]I. Drago, D. De Stefani, R. Rizzuto, and T. Pozzan, "Mitochondrial Ca^{2+} uptake contributes to buffering cytoplasmic Ca^{2+} peaks in cardiomyocytes," Proc. Natl. Acad. Sci. U.S.A. **109**, 12986–12991 (2012).
[56]G. S. Williams, L. Boyman, A. C. Chikando, R. J. Khairallah, and W. J. Lederer, "Mitochondrial calcium uptake," Proc. Natl. Acad. Sci. U.S.A. **110**, 10479–10486 (2013).